Pergamon

Int. J. Heat Mass Transfer. Vol. 37, No. 8, pp. 1257–1268, 1994

0017–9310/94 $7.00 + 0.00

Numerical simulation of fully developed flow in a curved duct of rectangular cross-section

M. D. SU
Department of Engineering Mechanics, Tsinghua University, Beijing 10084, China

and

R. FRIEDRICH
Technische Universität München, Germany

(*Received* 20 *June* 1992 *and in final form* 28 *September* 1993)

Abstract—The fully developed laminar and turbulent flows in curved ducts of rectangular cross-section are simulated numerically. The laminar flow is simulated with direct solution of Navier–Stokes equation and its results are compared with other numerical and experimental results. The turbulent flow is simulated with large eddy simulation (LES), in which Schumann's SGS-modelling is used. The computational results are presented and compared with Hur's (1990) results, which is accomplished by means of the statistic turbulent modelling.

1. INTRODUCTION

THE FLOWS in curved ducts of the rectangular cross-section are encountered in many engineering problems, for example, heat exchangers, fluids transport piping system, chemical reactors, meandering rivers and other apparatus, equipment or devices. So they are a topic of great interest to the engineering community.

Flows in ducts with various cross-sectional shapes have been the focus of numerous investigations in the past. Using the perturbation method, Dean [1–2] solved analytically the NS equation for fully-developed laminar flow in a curved pipe. He found that the dynamical similarity of the flow depends on a dimensionless parameter, which is now known as the Dean number De ($= Re\sqrt{(a/R)}$), where Re is the Reynolds number with bulk velocity, a the radius of pipe, and R the radius of curvature. In recent years, the use of numerical techniques to solve NS equations has considerably extended the knowledge of curved flow. In order to solve the equations of motion for fully developed laminar flow in a curved duct of rectangular cross-section, many numerical procedures have been reported [3–8].

Most flows encountered in many engineering problems, are turbulent. There were numerous investigations of the turbulent flow in straight and curved ducts. The results of investigation can be individed into two broad categories : experiments and numerical predicts. The case of the developing turbulent flow in curved ducts has been investigated in detail [9–14] through experiments and calculations. The computational analysis of the developing turbulent flow in curved square ducts has been also conducted [15–18]. We note that most numerical predictions are made with the solution of the three-dimensional time averaged Navier–Stokes equations incorporating a turbulent model based on two-equation or algebraic stress model. The flow is a developing turbulence. Recently, Hur *et al.* [19] have investigated numerically the fully developed turbulence in straight and curved ducts.

Recent advances in computational fluid dynamics, however, have opened a new way to fully three-dimensional computation of this type of flow. This provides the possibility of detailed and accurate flow predictions.

Because of the complexity of the flow in curved duct, it is necessary to simplify the mathematical description of this flow. Here a mathematical model of the fully-developed flow is used. Although it may be evident that this model cannot serve as a model of the flow in a real curved duct of rectangular cross-section, the results of simulation justify a qualitive analyses of the mechanism of main velocity redistribution due to the secondary flow in curved channels on the basis of this relatively simple and well-documented flow case. This flow case allows for the numerical solution of the complete unsteady NS equation in laminar flow and the filtered NS equation (basic equation of LES) for turbulence without extremely high computer costs. So that, in this work, as a first step of numerical simulations of turbulence in curved ducts, the fully-developed flow in curved ducts of rectangular cross-section is investigated with the numerical simulation. The present work consists of two parts : numerical simulation of the laminar flow

NOMENCLATURE

A_m trigonal matrix of order m
$\Delta A_1, \Delta A_2, \Delta A_3$ side surface elements of grid
De Dean number
D_h hydraulic diameter of duct section
E kinetic energy, $\frac{1}{2}(u^2+v^2+w^2)$
$\tilde{E}$ SGS kinetic energy, $\frac{1}{2}(\tilde{u}^2+\tilde{v}^2+\tilde{w}^2)$
$\mathbf{e}_1, \mathbf{e}_2, \mathbf{e}_3$ unit vectors in the three directions of the orthogonal curvilinear coordinate system
$\bar{f}$ volume averaged (filtered) value of f
f' $f-\bar{f}$
$\tilde{f}$ $f-\langle f\rangle$
$G(\mathbf{r}|\mathbf{r}')$ filter function
h_1, h_2, h_3 Lamé coefficients of the orthogonal curvilinear coordinate system
N_1, N_2, N_3 numbers of cells in three directions
p pressure
Re Reynolds number, $U_b L/\nu$
R radius of inner wall of curved duct or channel
S_{ij} components of strain rate tensor
U_b bulk velocity
v_1, v_2, v_3 velocity components in an orthogonal curvilinear coordinate system
${}^{\Delta V}\bar{v}_j$ velocity v_j averaged over grid volume
${}^{\Delta A_i}\bar{v}_j$ velocity v_j averaged over side-surface ΔA_i
$\tilde{v}_1, \tilde{v}_2, \tilde{v}_3$ Reynolds' velocity fluctuations
x_1, x_2, x_3 coordinations of the orthogonal curvilinear coordinate system
$\bar{V}$ volume
$\Delta\bar{V}$ grid volume
$\Delta\bar{V}_i$ grid volume staggered in i-direction.

Greek symbols
Δ length scale of grid, $\sqrt[3]{h_1h_2h_3\Delta x_1\Delta x_2\Delta x_3}$; Laplace operator
μ dynamic viscosity
ν kinematic viscosity
ν_T 'turbulent' viscosity
ρ density; distance
τ_{ij} components of stress tensor $\{\tau\}$ here, i indicates the direction normal to the surface in which the component lies and j represents the direction of the component.

Other symbols
∇ nabla operator
$\langle\cdot\rangle$ time-averaged value
$(\tilde{\ })$ Reynolds' fluctuation.

Superscripts
$+$ positive direction
$-$ negative direction.

with direct solution of Navier–Stokes (NS) equations and of the turbulent flow with large eddy simulation (LES).

2. BASIC EQUATIONS AND NUMERICAL METHOD

The continuity equation and Navier–Stokes equations are satisfied in the viscous flow, for both laminar and turbulent cases. Here it is assumed that the fluid is incompressible and Newtonian. The convection, which is produced with difference of temperature, is not considered, and so the equation of energy is ignored.

With the large eddy simulation method, all physical quantities f, e.g. velocity, pressure, etc., are divided into two parts: large scale part $\bar{f}$ and small scale part f'. Here the box filter is used:

$$G(\mathbf{r}|\mathbf{r}') = \begin{cases} \dfrac{1}{\Delta_1\Delta_2\Delta_3} & -\dfrac{\Delta_i}{2} \leqslant x_i \leqslant \dfrac{\Delta_i}{2} \\ 0 & |x_i| > \dfrac{\Delta_i}{2} \quad x_i = (\mathbf{r}-\mathbf{r}')_i \end{cases} \quad (i = 1, 2, 3). \tag{1}$$

The filtering value of f is denoted as $\bar{f}$ and calculated from

$$\bar{f} = \int_{-\infty}^{+\infty} G(\mathbf{r}|\mathbf{r}')\cdot f(\mathbf{r}')\mathrm{d}\mathbf{r}' \tag{2}$$

and

$$f = \bar{f}+f'. \tag{3}$$

$\bar{f}$ is called large scale part of f and f' its small scale part. After the definition of the box filter we have

$$\overline{fg} = \bar{f}\bar{g}+\overline{f'g'}. \tag{4}$$

It is easy to prove, that the value of $\overline{f'g'}$ will be $O(\delta^2)$, if the variations of f and g are smooth (for example, the variations of the velocities in the laminar flow); and it will be comparable with $O(1)$ if f and g vary suddenly. The basic equations of LES can be obtain by means of filtering NS-equation and are written in the following form:

Continuity equation

$$(\Delta A_1^{+\Delta A_1^+}\overline{v_1}-\Delta A_1^{-\Delta A_1^-}\overline{v_1})+(\Delta A_2^{+\Delta A_2^+}\overline{v_2}-\Delta A_2^{-\Delta A_2^-}\overline{v_2}) + (\Delta A_3^{+\Delta A_3^+}\overline{v_3}-\Delta A_3^{-\Delta A_3^-}\overline{v_3}) = 0 \tag{5}$$

Momentum equation

$$\Delta\bar{V}\frac{\partial}{\partial t}\Delta\bar{V}_i\overline{v_i}+\sum_{l=1}^{3}(\Delta A_l^{+\Delta A_l^+}\overline{v_l}^{\Delta A_l^+}\overline{v_i}$$

$$-\Delta A_l^{-\Delta A_l^-}\overline{v_l}^{\Delta A_l^-}\overline{v_i})+(\Delta A_l^{0\Delta A_l^+}\bar{p}-\Delta A_l^{0\Delta A_l^-}\bar{p})$$

$$-\sum_{l=1}^{3}(\Delta A_l^{+\Delta A_l^+}\overline{\tau_{li}^*}-\Delta A_l^{-\Delta A_l^-}\overline{\tau_{li}^*})$$

$$+\sum_{l=1}^{3}\left\{\left[\frac{\Delta x_l}{2}\Delta A_l^+\left(\frac{\partial h_i}{h_i\partial x_i}\right)_{\text{cen}}({}^{\Delta A_l^+}\overline{v_l}^{\Delta A_l^+}\overline{v_l}\right.\right.$$

$$-{}^{\Delta A_l^+}\overline{\tau_{li}^*}+{}^{\Delta A_l^+}\bar{p})$$

$$+\frac{\Delta x_l}{2}\Delta A_l^-\left(\frac{\partial h_i}{h_i\partial x_i}\right)_{\text{cen}}({}^{\Delta A_l^-}\overline{v_l}^{\Delta A_l^-}\overline{v_l}-{}^{\Delta A_l^-}\overline{\tau_{li}^*}+{}^{\Delta A_l^-}\bar{p})\Big]$$

$$-\left[\frac{\Delta x_i}{2}\Delta A_i^+\left(\frac{\partial h_i}{h_i\partial x_i}\right)_{\text{cen}}({}^{\Delta A_i^+}\overline{v_i}^{\Delta A_i^+}\overline{v_l}-{}^{\Delta_i^+}\overline{\tau_{il}^*}+{}^{\Delta A_i^-}\bar{p}\delta_{il})\right.$$

$$+\frac{\Delta x_i}{2}\Delta A_i^-\left(\frac{\partial h_i}{h_i\partial x_i}\right)_{\text{cen}}({}^{\Delta A_i^-}\overline{v_i}^{\Delta A_i^-}\overline{v_l}$$

$$\left.\left.-{}^{\Delta A_i^-}\overline{\tau_{il}^*}+{}^{\Delta A_i^-}\bar{p}\delta_{il})\right]\right\}=0 \tag{6}$$

$${}^{\Delta A_i}\overline{\tau_{ij}^*}=\frac{1}{Re}{}^{\Delta A_i}\overline{S_{ij}}-{}^{\Delta A_i}\overline{v_i'v_j'} \tag{7}$$

$$S_{ii}=2\left[\frac{1}{h_i}\frac{\partial v_i}{\partial x_i}+\frac{v_j}{h_ih_j}\frac{\partial h_i}{\partial x_j}+\frac{v_k}{h_ih_k}\frac{\partial h_i}{\partial x_k}\right]\quad\text{for}\quad i=i$$

$$S_{ij}=\frac{1}{h_j}\frac{\partial v_i}{\partial x_j}+\frac{1}{h_i}\frac{\partial v_j}{\partial x_i}-\frac{v_i}{h_ih_j}\frac{\partial h_i}{\partial x_j}-\frac{v_j}{h_ih_j}\frac{\partial h_j}{\partial x_i}\quad i\neq j$$

where $i=1,2,3$ and $j=\text{mod}(i,3)+1$, $k=\text{mod}(i+1,3)+1$.

Because of the sudden variation of velocities in the turbulent flow the value ${}^{\Delta A_i}\overline{v_j'v_k'}$ cannot be ignored. To closure the equation (2) in the numerical simulation of turbulent flow, we need model for terms: ${}^{\Delta A_i}\overline{v_j'v_k'}$, which are introduced with the fine-structure of turbulence. These terms are known as quasi-Reynolds stresses or subgrid scale (SGS) stresses, because they reflect the exchange of the momentum between difference parts in fluid. Here Schumann's model is used, which was developed on the basis of the vortex–viscous conception and the statistic turbulence theory by Schumann and described in detail in his Ph.D. Thesis [20].

Equations (1) and (2) are basic equations of turbulent flow in LES. In the laminar flow the terms $\overline{v_i'v_j'}$ in equation (2) are of second order of grid-scale and can be ignored; then the equation (2) becomes integral form of NS equation and can be used as principal equation of the numerical simulation of laminar flow.

Here ΔA_i^+ and ΔA_i^- are the sideward surfaces with subscript i denoting the normal direction of the surface and the superscripts + and − denoting the positive and negative side surfaces of the grid volumn respectively.

Figure 1 shows the geometry and the coordinate

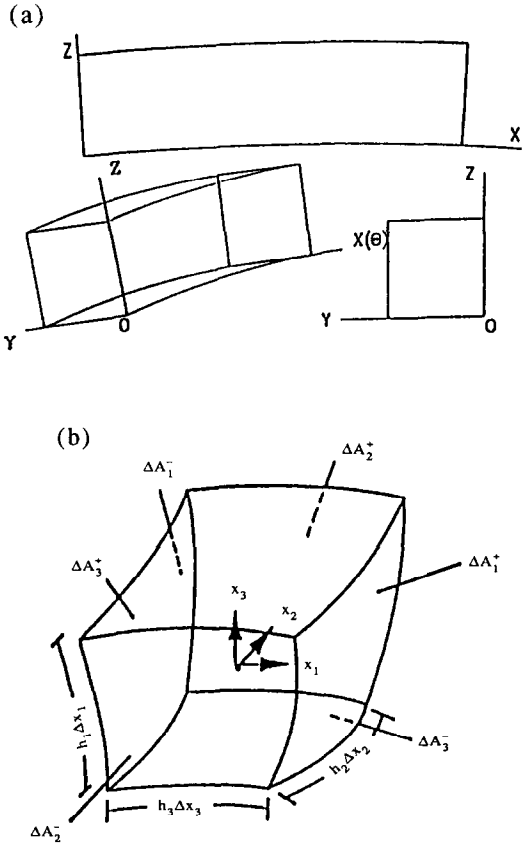

FIG. 1. Sketch of flow field and volume of grid.

system for a curved duct with rectangular cross-sections. R is the curvature radius of the inner wall. x_1 is the coordinate along the curved inner wall of the duct. x_3 is the coordinate normal to the inner wall and x_2 is the cross direction, which is parallel with inner wall and normal to the two other coordinates x_1, x_2. They constitute a right-hand coordinate system.

Boundary condition

Because the fully developed flows are considered, so that in x_1 direct, there is periodic condition for velocities v_1, v_2, v_3 and fluctuating p_1, which is a part of pressure p and it satisfies

$$p=p_0+p_1 \tag{8}$$

where $p_0=(\partial p_0/\partial x_1)\cdot x_1$ and $\partial p_0/\partial x_1$ is a given constant. On the wall, the adherent condition is used, e.g. $\mathbf{V}=0$ on the wall. Besides, $\partial p/\partial n=0$ on wall is assumed, n is the normal direct of the wall.

In the turbulent flow, when the point, at which the velocity is defined, is at the wall, then the velocity is equal to zero. Otherwise the logarithmic law is used.

The initial velocity field should satisfy the continuous equation. In order to solve equations (2) and (3), the following techniques are used: the finite difference method in time and the Marker and Cell (MAC) method, the spectral method for solving Poisson equation of the pressure.

It must be pointed that the transformation in the x_1 direction is Fourier transformation and can be completed directly with Fast Fourier Transformation (FFT). The transformation in the x_2 direction is Gauss–Chebyshev transformation and cannot be completed with FFT, but the FFT can be used also after reordering the coefficients of GC transformation. The detailed process is described by Su [21].

3. NUMERICAL RESULTS AND CONCLUSION

Laminar flow

The above presented method is used to calculate three fully developed laminar flows in curved ducts with different rectangular cross-sections. The radius of central line of curved duct is $5.5L$, the sides of cross-section are (1) $a = L$, $b = L$; (2) $a = 2L$, $b = L$; (3) $a = 0.5L$, $b = L$, where a is width of cross-section and b is its height. L is a characteristic length. The Reynolds number is defined with the characteristic length L, the kinematic viscosity ν and the bulk velocity U_m. Dean's number is defined with formula $De = D_h U_m/\nu$, where $D_h = 2ab/(a+b)$ is the hydraulic diameter. The number of grid points in cross-section is 32×32.

At first, the flow in a curved duct with square cross-section is discussed. The contours of the axial flow velocity and streamlines of the secondary motion with different De numbers are displayed and compared with De Vriend's results in Fig. 2. It is easy to see that the distribution of the axial flow velocity is skewed in the radial direction due to the curvature of the duct. With the increase of the bulk velocity (or the Dean and Reynolds numbers), the position of the maximum velocity is shifted to the outer wall. It appears twice, namely to the right and left of the symmetry plane.

When the Dean number is low (e.g. less than 101), the pattern of the secondary flow contains two cells, symmetrically arranged with respect to the $y = 0.5$-plane. In this case, the contribution of the secondary flow to the distortion of the axial velocity consists of two parts, namely a radial and a cross velocity component. When a fluid particle moves along a curved path, it is driven to the outer wall by a centrifugal force. In the central part of the duct, the largest radial velocities appear, with magnitudes as large as $\sim 10\%$ of that of the axial velocity. In the vicinity of the side walls, however, the centrifugal forces are reduced by viscosity effects and can thus be compensated by continuity effects. The result is a secondary flow towards the inner wall on both side walls. Thus the vortex pair of secondary flow is formed in the cross-section. The fluid particles move from the center of the duct to the left- and right-corners of the outer wall, then along the side walls to the inner wall, and finally return to the central plane along the inner wall. The secondary flow brings the momentum of the fluid from the center to the outer side of the duct and changes the distribution of the axial velocity. The tendency of the secondary flow is to reduce the cross-averaged axial velocity near the inner wall and to increase it near the outer wall.

As the Dean number increases, however, the convective transport of momentum away from the side walls is mainly radial, outward in the central part of

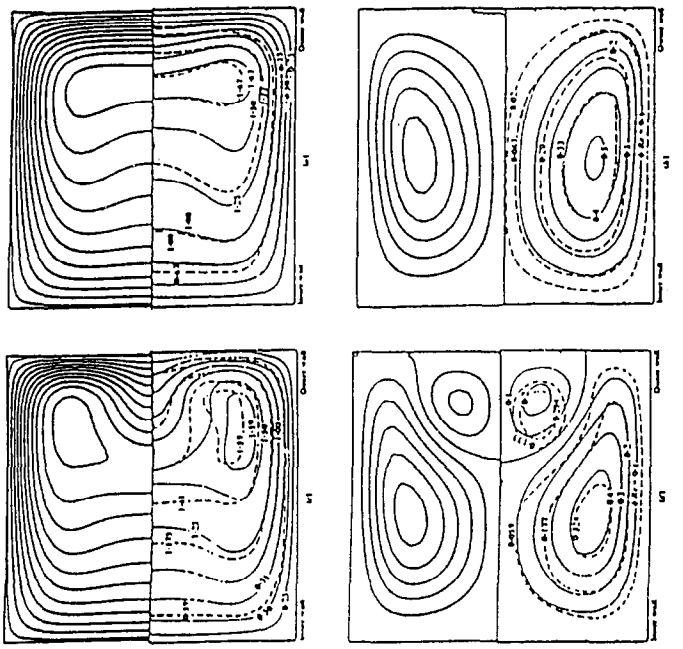

FIG. 2. Comparison between the present result and De Vriend's result: left, present results; right, De Vriend's result; top, $De = 94.8$; below, $De = 107.6$.

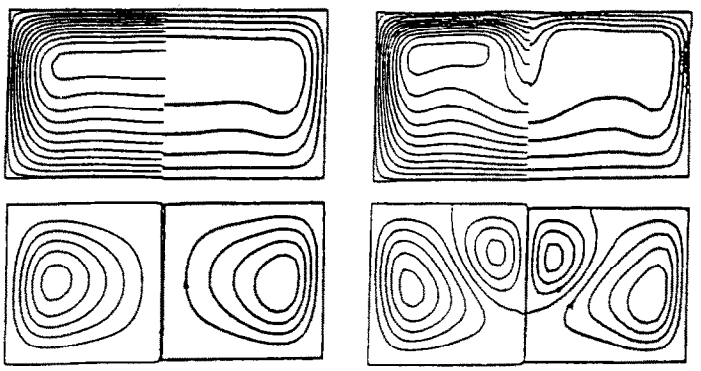

FIG. 3. Comparison between the present result (left) and Hur's result (for aspect ratio $a/b = 2.0$) (top, contours of main velocity; below, streamlines of secondary flow).

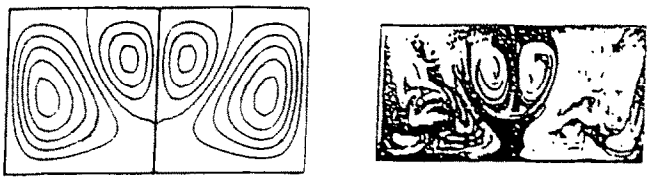

FIG. 4. Comparison between the present result and Sugiyama's result (for aspect ratio $a/b = 2.0$, $Re = 575.37$, $De = 150.45$).

the cross-section and inward in the side part of the cross-section, such that there is a net outward momentum transport. With the side shear stress as a damping factor, this net outward transport gives rise to a retarded outward expansion of the low-velocity region near the inner wall. The velocity peak is shifted against the outer wall, where it is partly damped by viscous forces. As a consequence, the axial velocity distribution tends to be skewed outwards and hence radial convection causes a flattening of the cross profile of the axial velocity, the fluid convected from further inside giving rise to a momentum deficit in the central part of the cross-section and the fluid convected from further outside causing a momentum surplus in the side part.

In flows of curved rectangular ducts, similar phenomena can be also found, see Figs. 3 and 4, respectively. In the first case, the ratio of width a to height b of the cross-section is 2. The result for this case is compared with Thangam and Hur [22] and the agreement is satisfactory (see Fig. 3). The present result corresponds to Sugiyama *et al.*'s [23] experimental result (see Fig. 4). In the second case, the aspect ratio is 0.5. The comparison with experimental data reported in ref. [23] shows good agreement (see Fig. 5).

Turbulent flow

Outline of computational example. The large eddy simulation of the fully developed turbulence in a curved duct was carried out under the parameters listed in Table 1.

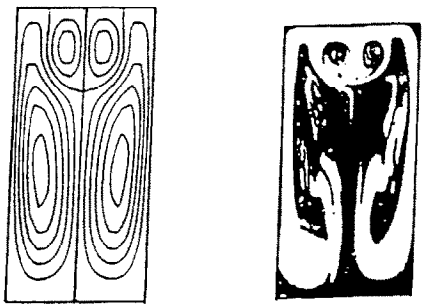

FIG. 5. Comparison between the present result and Sugiyama's result (for aspect ratio $a/b = 0.5$, $Re = 656.71$, $De = 221.20$).

Table 1.

	Case I	Case II
Reynolds number		
$Re_b = HU_b/\nu$	69 000.0	69 000.0
Comp. domains		
Length	$4H$	$4H$
Height	H	H
Width	$B = H$	$B = H$
Ratio of radius to height of duct		
Grid numbers		
$N_1 \times N_2 \times N_3$	$64 \times 32 \times 32$	$256 \times 64 \times 64$
Time-step number	42 000	21 800
CPU (hr)	22	182
Time increment		
$\Delta t = (\Delta T U_b/H)$	0.010	0.005

The numerical integration of the basic equations leads to 'wiggles', which change the pattern of the secondary flow in the cross-section of the curved duct and lead to unphysical distributions of the mean axial velocity. A consequence of these wiggles is that two small recirculation zones disappear. The 'wiggles phenomenon' occurs also in that of other authors [24, 25]. From the discussion in Roache's book (1982) it follows that 'wiggles' are an inherent feature of central difference schemes in space and are due to insufficient resolution. Therefore we try an upwind difference scheme. However, the experiences show: the 'wiggles' cannot be eliminated by the upwind difference scheme with high-order accuracy because it has too small damping; when an upwind difference scheme with second-order accuracy is used, the 'wiggles' and the turbulence are eliminated simultaneously due to the too large damping of the difference scheme. Usually, finer grids help to reduce the effect of 'wiggles'.

A mixed difference scheme with second-order accuracy is developed [21]. It can be written in the following form:

$$L = (1-\theta)\times L_2^{\mathrm{c}} + \theta \times L_2^{\mathrm{u}} \tag{9}$$

where L represents a finite difference operator, subscript 2 indicates second-order accuracy and superscripts u/c upwind-/central-schemes, respectively. The parameter θ is defined by:

$$\theta = \min\left\{1.0, \frac{|f_{-1} - 2\times f_0 + f_1|}{|f_{-1}| + 2\times|f_0| + |f_1|}\right\} \tag{10}$$

where f is one of the time averaged velocity components. The selection depends on which velocity component is calculated in the difference scheme. It is clear that the value of θ will be close to 1.0 if 'wiggles' are strong, and the upwind difference scheme will play a leading role in the mixing scheme. If 'wiggles' are weak, the central scheme will play the main role. In the present numerical simulation the 'wiggles' are overcome at last. Therefore the central difference scheme is used in fact when the 'wiggles' are overcome.

It must be noted that, till now, we have not found any reported experiment which treats the fully developed turbulence in curved ducts, despite there being many experiments which treat developing flow in curved ducts. However, the fully developed flow has been predicted numerically by Hur *et al.* [19] with a turbulence model. Therefore, the following results are compared with Hur's numerical results.

Distribution of the statistically averaged velocities. The fully developed averaged turbulent flow in a curved duct is steady. The contour of $\langle u\rangle$ in cross-section of duct is shown in Fig. 6(a), from which one can find that the mean turbulent flow is similar to the laminar flow (see Fig. 2). As De Vriend [5] pointed out, there are points of qualitative resemblance between the two flow types. Firstly, in turbulent flow

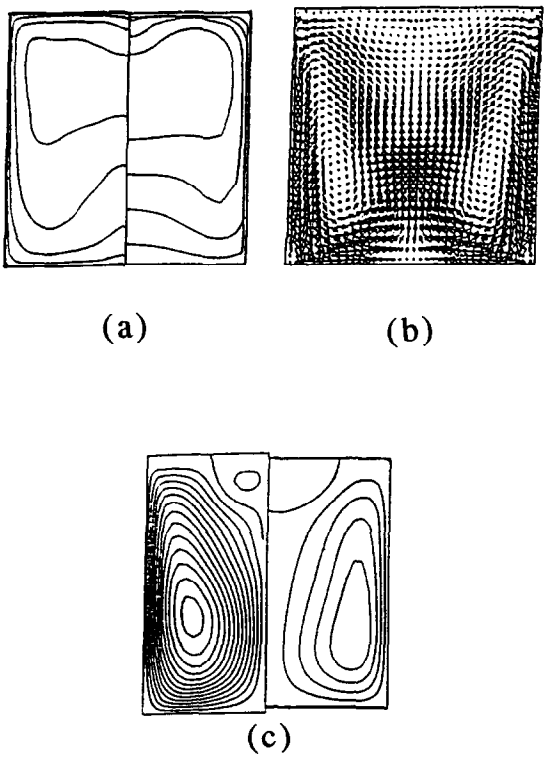

FIG. 6. Comparison of pattern of the secondary flow in curved duct: (a) contour of $\langle u\rangle$ in cross-section; (b) vectors of velocities in cross-section; (c) streamline of the secondary flow. Note: the right in (a) and (c) are Hur *et al.*'s results [19], others are present numerical result.

the convective exchange of momentum due to the velocity fluctuations can be modelled using the analogy of molecular diffusion (Boussinesq hypothesis) and the coefficient of turbulence viscosity in such models, though varying over the flow field, can be considered as a constant and therefore it qualitatively corresponds to the molecular viscosity. Some researchers suppose that the turbulent viscosity is 50–100 times the molecular viscosity. In addition, both laminar and turbulent flow in curved conduits show the characteristic helical flow pattern, caused by the same mechanism in either case. Besides, the redistribution of the main velocity along a bend shows the same features for laminar and turbulent flow. The present results support the above viewpoints, and, in addition, the above-mentioned cases will be between 490 and 980 and the corresponding equivalent Dean number will be between 88 and 176. Comparing the present result with Hur's result [19] (see Fig. 6(a)), it can be confirmed that both results agree qualitatively. The positions of maximum value of $\langle u\rangle$ shift outwards and sidewards.

Secondary flow in the curved square duct

As already mentioned, there is a mean secondary flow in the fully developed turbulent flow of a curved duct. There are some points of qualitative resemblance

between laminar and turbulent flows in curved ducts, namely where the origin of the mean secondary flow is concerned. The streamlines and projections of the mean velocity vector into a cross-section and a comparison between them and Hur *et al.*'s result [19] is shown in Fig. 6(c), from which one can conclude that the mean secondary flow in the curved duct is well reflected in the present numerical simulation.

It should be emphasized that the intensity of the mean secondary flow is small and the small recirculation region near the outer wall contains even weaker fluid motions, which are easily eliminated by a careless computation. One can say that it is an important criterion of correctness of the numerical simulation of such flows when the secondary motion is described correctly. Because of the different mechanisms that generate secondary flows in straight and in curved ducts, the distribution patterns of time-averaged main velocity $\langle u \rangle$, cross velocities $\langle v \rangle$, $\langle w \rangle$, turbulent kinetic energy $\langle \tilde{E} \rangle$ and components of the Reynolds stress tensor $\langle \tilde{u}\tilde{u} \rangle$, $\langle \tilde{u}\tilde{v} \rangle$, ... are different.

From Fig. 6 one can find that the pattern of the time-averaged main velocity in a curved duct is symmetrical with only one symmetry axes. Besides, the position with the maximum main velocity moves outward and sideward due to the centrifugal effects. As we know, the secondary flow leads to the exchange of fluid momentum and turbulence kinetic energy between the different parts of the curved duct and the distributions of averaged velocities, turbulence kinetic energy and Reynolds stresses. In Fig. 7 the contours of Reynolds stresses $\langle \tilde{u}\tilde{u} \rangle$, $\langle \tilde{v}\tilde{v} \rangle$, $\langle \tilde{w}\tilde{w} \rangle$, $\langle \tilde{u}\tilde{v} \rangle$, $\langle \tilde{u}\tilde{w} \rangle$, $\langle \tilde{u}\tilde{w} \rangle$, turbulence energy $\langle \tilde{E} \rangle$, in the cross-section of the curved channel and the curved duct are compared. Because of the unsymmetry of their distributions in the z-direction, the profiles along both y- and z-directions are shown. From these figures of $\langle \tilde{u}\tilde{u} \rangle$, $\langle \tilde{v}\tilde{v} \rangle$, $\langle \tilde{w}\tilde{w} \rangle$, $\langle \tilde{E} \rangle$, one finds that the intensity of the turbulence kinetic energy is strengthened in the vicinity of walls, especially in the vicinity of the outside wall due to the effect of the duct curvature. However the shape of these distributions is not different essentially from that in the straight duct. Comparing those pictures of $\langle \tilde{u}\tilde{v} \rangle$, $\langle \tilde{u}\tilde{w} \rangle$, $\langle \tilde{v}\tilde{w} \rangle$, with that in the straight duct, the essential discrepancy can be seen clearly.

It is clear too that the distribution of components

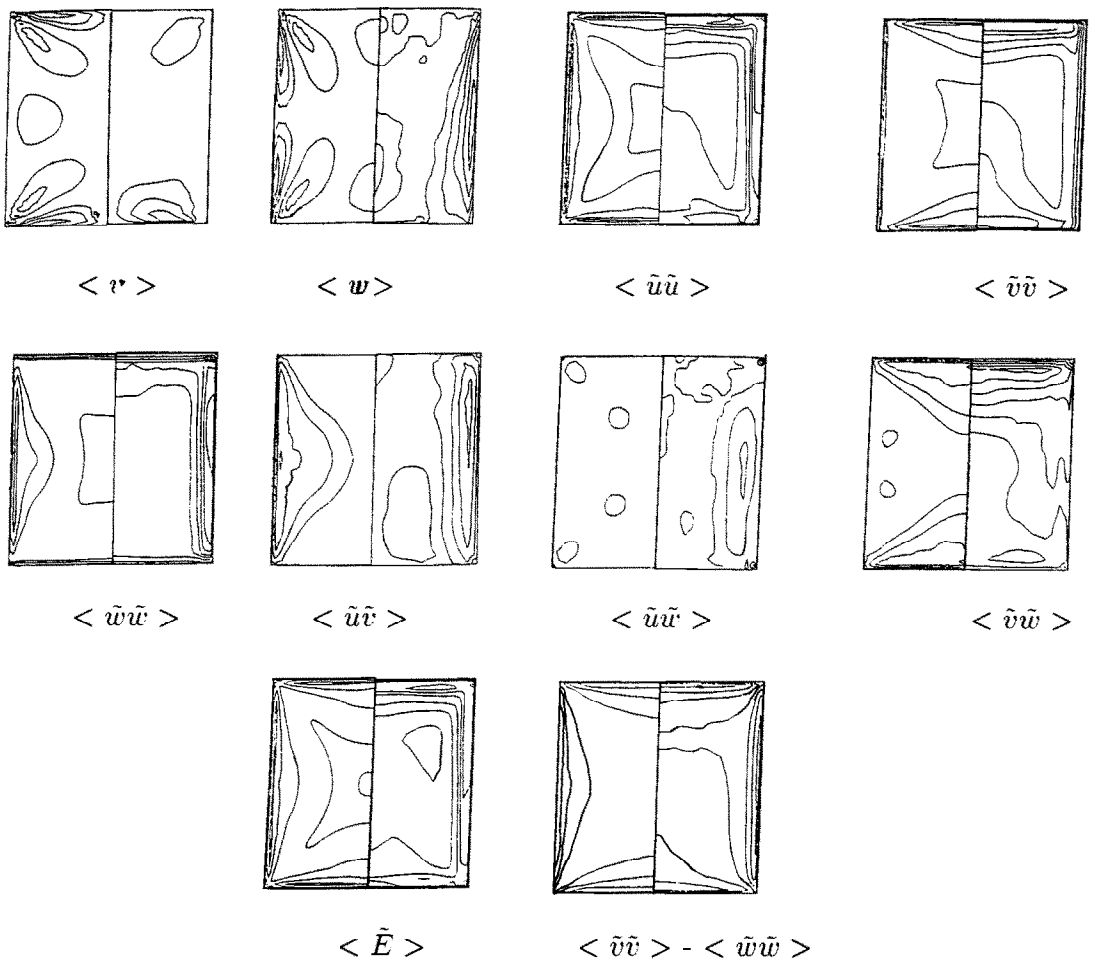

FIG. 7. Comparison of contours; left: in straight duct; right: in curved duct.

of Reynolds stress tensor are affected not only by curvature of the duct, but also by the side walls. It can be confirmed that the changes of distribution of $\langle\tilde{u}\tilde{u}\rangle$,... are reduced by the secondary flow. Comparing their contours $\langle\tilde{u}\tilde{u}\rangle$, $\langle\tilde{v}\tilde{v}\rangle$, $\langle\tilde{w}\tilde{w}\rangle$, $\langle\tilde{E}\rangle$ in the curved duct and those in the straight duct, the contour of $\langle\tilde{v}\tilde{v}\rangle-\langle\tilde{w}\tilde{w}\rangle$ is displayed in Fig. 7. It should be pointed out that the value of $\langle\tilde{v}\tilde{v}\rangle-\langle\tilde{w}\tilde{w}\rangle$ is small and near zero in the central part of the straight duct. However, the unsymmetry of the contour in the curved duct is produced by the duct curvature.

Comparing the results of LES in the curved duct and in the straight duct, it makes clear that the change of the pattern of the secondary flow and the distribution variations of mean velocities and Reynolds stresses are reduced not only by curvature of duct or channel but also by the existence of side walls. It can be concluded that the change in the turbulence model by means of introducing some special coefficients with curvature influence can reflect the action of curvature only partially and be available only to simple turbulent flow, for example in a 2D curved channel. However, the present large eddy simulation method can reflect the influence of curvature of the duct as well as the side walls. The present example shows that the method of LES is a general method for numerical simulation of complex turbulent flow.

Instantaneous structure of turbulence in the curved duct

The fully developed turbulence in the curved square duct is complex turbulence and the analysis of turbulence structure is a difficult and complex job. Here only a primary analysis was carried out.

Figure 8 shows the contours of instantaneous fluctuate velocity $\tilde{v}$ at different longitudinal sections (i.e. (x, z)- planes or y = const. planes) respectively. It can be found that the distinct structure with inclination angle ($\sim 25^\circ$) to the adjacent wall in the contour of $\tilde{v}$ at $y = H/4$. These contours have denser structure near the outside wall than that near the inside wall. This means the turbulence is strengthed by the convex wall and weakened by the concave wall. Figure 9 shows the contours of three components of instantaneous vortex vector and the abovementioned phenomenon was clearly displayed too.

Figure 10 shows the projection of instantaneous fluctuate velocity vector into longitudinal sections at different positions (i.e. different planes with y = const.). The distinct vortex structures are displayed in Fig. 11, which shows the projection of instantaneous fluctuate vorticity vector into longitudinal sections at the same positions as in Fig. 10. One can find the turbulence motions of fluid are not so disorderly as one thinks. There are some surges and some circular structures are displayed faintly. These surges and faint circular structure are unstable and varied. It can be confirmed from these figures that the coherent structure exists in the fully developed turbulence of the curved duct and should be researched further.

In the fully developed turbulent flow in the curved duct one can find some large vortex lines (tubes), some of them are displayed in Fig. 12, where one sees that there are some horse-shoe shape vortex lines (tubes) near both convex and concave walls. However, Fig. 12 shows some ring or half-ring vortex lines and most of them concentrate in the outside corners (i.e. near the concave wall). This phenomenon has not been found in the fully developed turbulent flow in the straight duct. Besides, the angles between the planes, in which the vortex lines lie, and their adjacent wall are near 90°: they are not near 45° as in the straight duct.

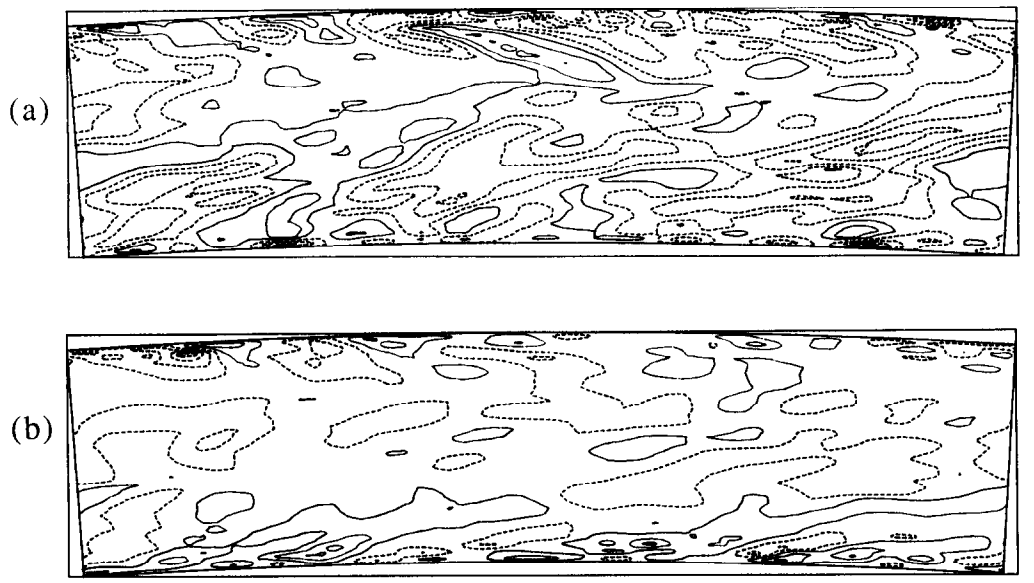

FIG. 8. Contours of instantaneous fluctuate velocity $\tilde{v}$: (a) $y = H/4$; (b) $y = H/8$.

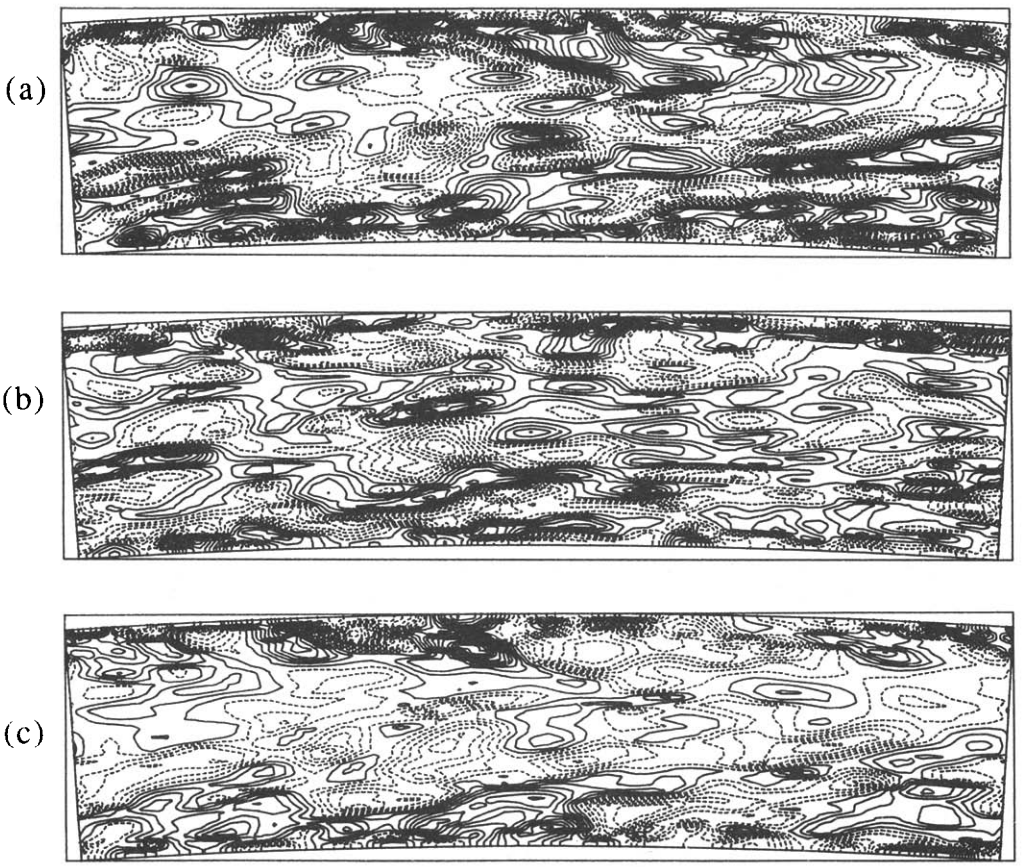

FIG. 9. Contours of instantaneous fluctuate vortex: $\tilde{w}_{,y}$. (a) $\tilde{w}_{,y}$; (b) $\tilde{w}_{,x}$; (c) $\tilde{w}_{,z}$.

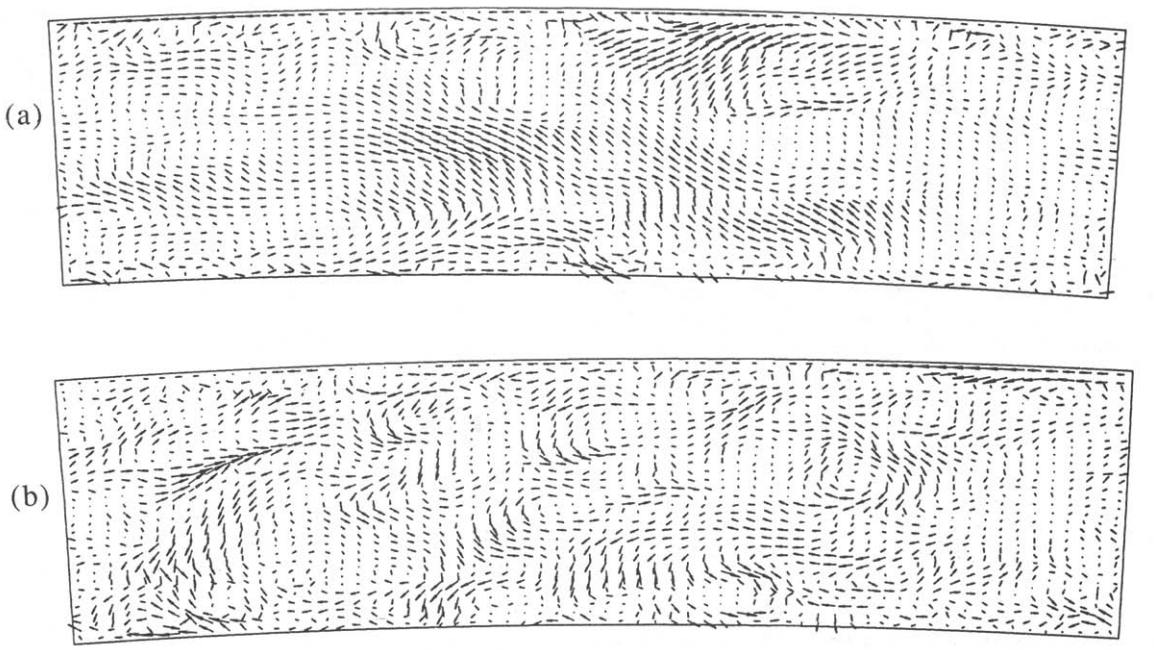

FIG. 10. Projection of instantaneous fluctuate velocity vector into (x, z)-planes: (a) $y = H/4$; (b) $y = H/2$.

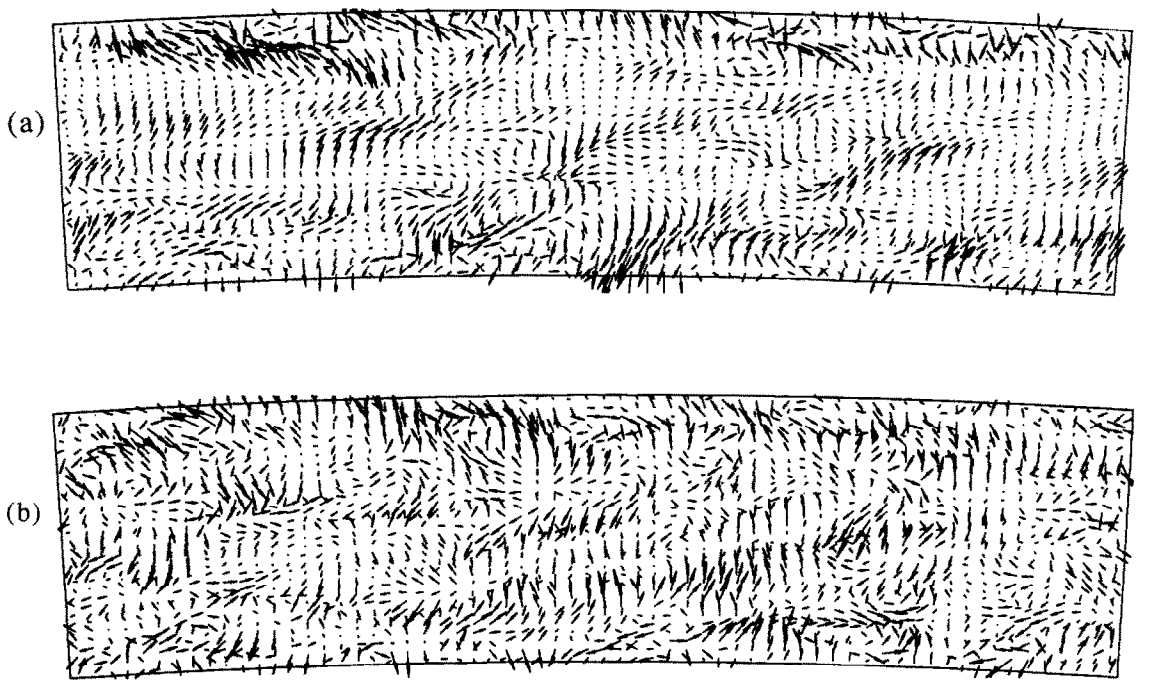

Fig. 11. Projection of instantaneous fluctuate vorticity vector into (x, z)-planes: (a) $y = H/4$; (b) $y = H/2$.

4. CONCLUSION

From the present discussion the following conclusions can be obtained:

1. The presented numerical data correctly reflect the influence of duct curvature on the distribution of axial flow and on the pattern of secondary motions. The relation between the Dean number and the pattern of the secondary flow is also correct and confirms the underlying physical mechanisms;

2. The three laminar flows in curved rectangular ducts with different aspect ratios have yielded results which agree well with experimental data reported in the literature;

3. In the numerical simulation there are some problems, which can influence or change the final results seriously. The 'wiggles phenomenon' is an important example: the pattern of secondary flow is changed seriously and the distribution of time-meaning velocity is not rational physically. In the present computation the 'wiggles phenomenon' is overcome finally with a mixing scheme. The numerical results show the effects of the duct curvature correctly.

4. The comparison between the present and Hur *et al.*'s results [19] of the time-average velocity and secondary flow show that the method of LES and the SGS-model are available to simulate numerically complex turbulences such as that in a curved duct.

5. The curvature influence of the turbulence is not so simple and cannot be described with a simple factor as in Bradshaw's model [26], because there are also some other factors such as the existence of side wall and so on. As the grids are small enough, the results of LES can reflect the curvature-effect automatically.

6. Some instantaneous structures of the turbulence in the curved duct are displayed, and make clear that there is some coherent structure in the turbulence, which should be analysed further.

Acknowledgement—The work reported here was sponsored by the Deutsche Forschungsgemeinschaft.

REFERENCES

1. W. R. Dean, The stream-line motion of fluid in a curved pipe, *Phil. Mag. S7* **5**, 673–695 (1928).
2. W. R. Dean, Fluid motion in a curved channel, *Proc. Roy. Soc. A* **121**, 402–420 (1928).
3. K. C. Cheng and M. Akiyama, Laminar forced convection heat transfer in curved rectangular channels, *Int. J. Heat Mass Transfer* **13**, 471–490 (1970).
4. K. C. Cheng, R. C. Lin and J. W. Ou, Fully developed laminar flow in curved rectangular channels, *Trans. A.S.M.E. I. J. Fluids Engng* **98**, 41–48 (1976).
5. H. J. De Vriend, Velocity redistribution in curved rectangular channels, *J. Fluid Mech.* **107**, 423–430 (1981).
6. B. Joseph, E. P. Smith and R. J. Adler, Numerical treat-

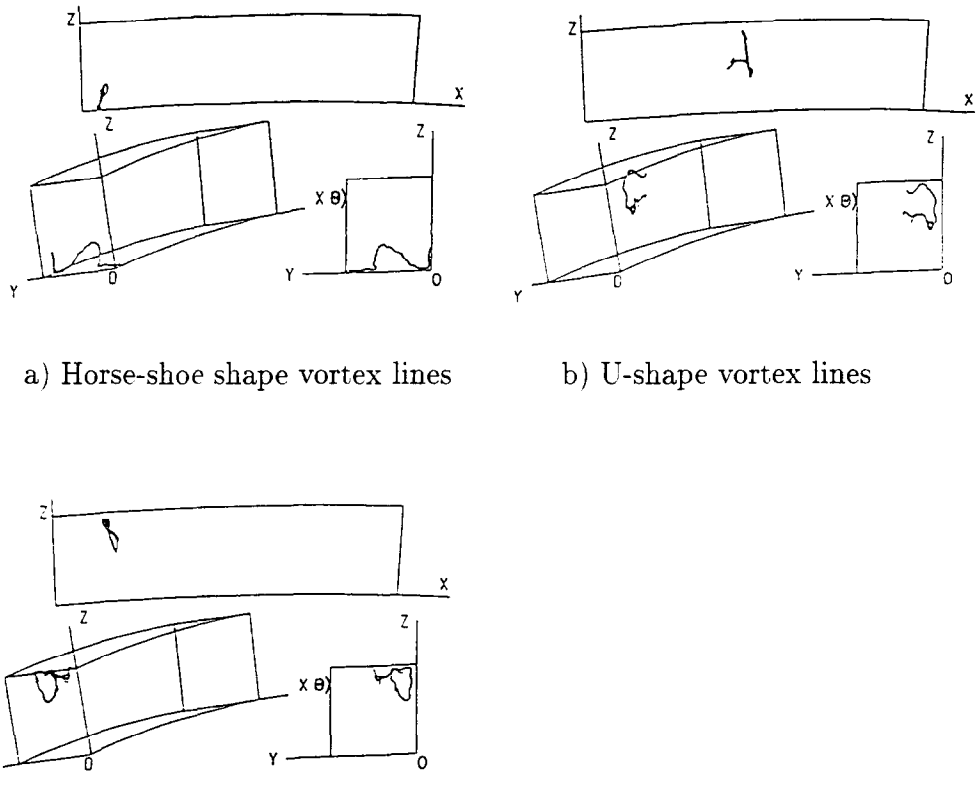

FIG. 12. Vortex lines in curved duct.

ment of laminar flow in helically coiled tubes of square cross-section. Part 1: Stationary helically coiled tubes. *A.I.Ch.E. Jl* **21**, 965–974 (1975).
7. Y. Mori, Y. Uchida and T. Ukon, Forced convective heat transfer in a curved channel with a square cross section, *Int. J. Heat Mass Transfer* **14**, 1787–1805 (1971).
8. N. Shiragami and I. Inoue, Fully developed and developing laminar velocity profiles in a rectangular bend, *J. Engng Fluid Mech.* **21**, 100–133 (1988).
9. M. P. Arnal, Investigation of developing laminar and turbulent flow in curved ducts, Ph.D. Thesis, University of California, Berkeley (1988).
10. S. M. Chang and J. A. C. Humphrey, Turbulent flow in a passage around 180° bend; an experimental and numerical study, Report F. M. 83-7, University of California, Berkeley (1983).
11. S. M. Chang, J. A. C. Humphrey and A. Modavi, Turbulent flow in a strongly curved U-bend and downstream tangent of square cross-sections, *Physico-Chemical Hydrodynamics* **4**(3), 243 (1983).
12. J. A. C. Humphrey, J. H. Whitelaw and G. Yee, Turbulent flow in a square duct with strong curvature, *J. Fluid Mech.* **103**, 443–463 (1981).
13. A. M. K. P. Taylor, J. H. Whitelaw and M. Yianneskis, Curved ducts with strong secondary motion: velocity measurements of developing laminar and turbulent flow, *ASME J. Fluid Engng* **21**, 965–974 (1982).
14. S. M. Chang, Measurement and calculation of developing turbulent flow in a U-bend and downstream tangent of square cross-section, Ph.D. Thesis, University of California, Berkeley (1983).
15. V. S. Pratap, Flow and heat transfer in curved ducts, Ph.D. Thesis, London University (1975).
16. Y. D. Choi, H. Iacovides and B. E. Launder, Numerical computation of turbulent flow in a square-sectioned 180° bend, *ASME J. Fluid Engng* **111**, 59–68 (1989).
17. V. S. Pratap and D. B. Spalding, Numerical computation of the flow in curved ducts, *Aeronaut. Q.* **26**, 219–228 (1975).
18. V. S. Pratap and D. B. Spalding, Fluid flow and heat transfer in three-dimensional duct flows, *Int. J. Heat Mass Transfer* **26**, 219 (1976).
19. N. Hur, S. Thangam and C. G. Speziale, Numerical study of turbulent secondary flows in curved ducts, *ASME J. Fluid Engng* **112**, 205–211 (1990).
20. U. Schumann, Ein Verfahren zur directen numerischen Simulation turbulenter Strömungen in Platten- und Ringspaltkanälen und über seine Anwendung zur Untersuchung von Turbulenzmodellen, Dissertation, Universität Karlsruhe, KFK 1854 (1973).

21. M. D. Su, Large-Eddy-Simulation vollentwickelter turbulenter Strömungen in Kanälen ohne und mit Längskrümmun, Dissertation, Technische Universität München (1993).
22. S. Thangam and N. Hur, Laminar secondary flows in curved rectangular ducts, *J. Fluid Mech.* **217,** 421–440 (1990).
23. S. Sugiyama, T. Hayashi and K. Yamazaki, Flow characteristics in the curved rectangular channels (visualization of secondary flow), *Bull. JSME* **26,** 964 (1983).
24. P. M. Gresho and R. L. Lee, Don't suppress the wiggles—they're telling you something!, *Comput. Fluids* **9,** 223–253 (1981).
25. H. Werner, Grobstruktursimulation der turbulenten Strömung über eine querliegende Rippe in einem Plattenkanal bei hoher Reynoldszahl, Dissertation, Technische Universität München (1991).
26. P. Bradshaw, Effects of streamline curvature on turbulent flow, *AGARDograph* **169** (1973).